Phononic Crystal Tunable via Ferroelectric Phase Transition

Chaowei Xu, Feiyan Cai, Shuhong Xie, Fei Li, Rong Sun, Xianzhu Fu, Rengen Xiong, Yi Zhang, Hairong Zheng, and Jiangyu Li

Tunable Phononic Crystal via Ferroelectric Phase Transition

Chaowei Xu,[1, 2, 3] Feiyan Cai,[2, 4] Shuhong Xie,[1] Fei Li,[2, 3] Rong Sun,[5] Xianzhu Fu,[5] Rengen Xiong,[6] Yi Zhang,[6] Hairong Zheng,[2, 3, 4, *] and Jiangyu Li[3, 7, †]

[1] *Key Laboratory of Low Dimensional Materials and Application Technology of Ministry of Education, School of Materials Science and Engineering, Xiangtan University, Xiangtan 411105, China*

[2] *Paul C. Lauterbur Research Center for Biomedical Imaging, Institute of Biomedical and Health Engineering, Shenzhen Institutes of Advanced Technology, Chinese Academy of Sciences, Shenzhen, 518055, China*

[3] *Shenzhen Key Laboratory of Nanobiomechanics, Shenzhen Institutes of Advanced Technology, Chinese Academy of Sciences, Shenzhen 518055, China*

[4] *Beijing Center for Mathematics and Information Interdisciplinary Sciences, Beijing, 100048, China*

[5] *Center for Advanced Materials, Shenzhen Institutes of Advanced Technology, Chinese Academy of Sciences, Shenzhen 518055, China*

[6] *Ordered Matter Science Research Centre, Southeast University, Nanjing 211189, China*

[7] *Department of Mechanical Engineering, University of Washington, Seattle, WA98195-2600, USA*

Phononic crystals (PC) consisting of periodic materials with different acoustic properties have potential applications in functional devices. To realize more smart functions, it is desirable to actively control the properties of PC on-demand, ideally within the same fabricated system. Here, we report a tunable PC made of $Ba_{0.7}Sr_{0.3}TiO_3$ (BST) ceramics, wherein a 20 K temperature change near room temperature results in 20% frequency shift in transmission spectra induced by ferroelectric phase transition. The tunability phenomenon is attributed to the structure-induced resonant excitation of A_0 and A_1 Lamb modes that exist intrinsically in the uniform BST plate, while these Lamb modes are sensitive to the elastic properties of plate and can be modulated by temperature in BST plate around Curie temperature. The study finds new opportunities for creating tunable PC and enables smart temperature-tuned devices such as Lamb wave filter or sensor.

---

*Corresponding author. hr.zheng@siat.ac.cn
†Corresponding author. jjli@uw.edu
C. Xu and F. Cai contributed equally to this work

I. Introduction

Phononic crystals (PC) consisting of periodic materials with diverse elastic modulus and mass density have great advantage in manipulating acoustic wave propagation and energy flow [1, 2]. By modulating the geometry and/or the constituent materials of the PC, many interesting phenomena can be realized, including band gap, negative refraction, and localized defect modes, which are promising for potential applications in cloaks, isolators, waveguides, sensors and filters. It is highly desirable to be able to tune the responses of PC on-demand during these applications, without the need to reconfigure the geometry or the constituents of PC, though large tunability is rather difficult to achieve in practice. To realize more versatile applications of PC, much of the effort focuses on developing tunable PC using smart structures [3-7] and materials [8-17], since their properties can be manipulated by external stimuli such as force, electric field, magnetic field, and temperature. For example, the mechanically triggered transformations of phononic band gaps is theoretically demonstrated through applied load [7]. Control of the elastic wave bandgaps in two-dimensional piezoelectric periodic structures by using different polarized directions is theoretically studied [8]. Using plane-wave-expansion method, Yeh theoretically investigated the elastic band structure of a two-dimensional PC made of electrorheological materials, and found that the electric field has a significant effect on the band gaps [9]. Similarly, through theoretical calculations, it was demonstrated that the band structure of PC made of magnetostrictive materials are tunable by external magnetic field [10-12]. Taking the magneto–electro–elastic coupling into account, the elastic wave propagation in two-dimensional magnetoelectroelastic PC is tuned by electric and magnetic fields [13, 14]. Tuning and switching the hypersonic phononic properties is realized through phase transitions of crystallization and melting, which can be tuned by temperature [15]. Recently, it was suggested that ferroelectric ceramics are suitable for tunable PC, since their acoustic velocities are sensitive to the temperature across Curie temperature (T_C) [18-21]. Nevertheless, most of these studies were theoretical in nature,

2

and focused on the obvious effects of external stimuli on the band structure of an infinite PC. Few experimental demonstration of tunable PC has been reported, and the anomalous properties of the pass band in a finite structure [18], which are much more interesting, have not been explored.

$Ba_{1-x}Sr_xTiO_3$ is a lead-free perovskite ferroelectric material that has been extensively investigated [22-24], and its T_C can be continuously modified by varying Ba/Sr ratio. For instance, T_C of $Ba_{0.7}Sr_{0.3}TiO_3$ (BST) is around room temperature of 298 K [25], across which large variations in material properties are observed due to ferroelectric phase transition, making it attractive for tunable applications. Here, we report a PC plate made of BST ceramic that is quite effective in exciting Lamb wave. By taking advantage of the acoustic transmission enhancement induced by Lamb wave in the PC plate [26, 27], thermal tuning of multi-peak acoustic transmission through the PC plate is demonstrated with 20% tunability in frequency. The tunability is based on the ferroelectric phase transition of BST that results in large variation of its acoustic properties across T_C [28], allowing us to tune the transmission of PC via temperature induced ferroelectric phase transition.

II. Experiment Methods

The BST ceramic was fabricated by conventional solid-state reaction technique and followed by viscous polymer processing (VPP) route. At the first, barium carbonate ($BaCO_3$, Aladdin, ≥99%), strontium carbonate ($SrCO_3$, Aladdin, ≥99%), and titania (TiO_2, Aladdin, ≥99%) powders were mixed in the appropriate molar ratios and ground thoroughly by an agate ball grinding mill for 10 hours. Secondly, the mixtures were calcined at 1100 ℃ for 2 hours in alumina crucibles opened to air after preloaded, and then griding it for another 10 hours. The ground powders were uniformly mixed with appropriate amount of polyvinyl alcohol (PVA, Sigma) solution (mass concentration: 3%) for granulating. Afterwards, the produced mixtures were compressed under the uni-axial pressure of 20 MPa into disks of 20 mm in diameter. In order to remove additive polymer, the pelletized were first heated up to

3

600 ℃ at a heating rate of 5 ℃/min. The samples were finally sintered at 1400 ℃ for 4 hours in alumina crucibles opened to air.

BST ceramic exhibits a dense grain structure with the grain size ranging from 10 μm to 30 μm, as seen from the scanning electron microscope (SEM, Nova NanoSEM 450, FEI) images of surface and cross-section in Fig. 1(a) and Fig. 1(b). X-ray diffraction (XRD, XD-3A, SHIMADZU) with Cu Kα radiation were used to characterize the phase structures and chemical component elements. The perovskite phase of the BST with tetragonal space group *P4mm* is confirmed by the XRD pattern at 293 K, as shown in Fig. 1(c) (black line), with which the lattice parameters are determined to be $a = b = 3.9853$ Å and $c = 3.9541$ Å. Only a slight shift in diffraction peak positions is observed in XRD pattern measured at 313 K (red line), and the corresponding lattice parameters are determined to be $a = b = c = 3.9754$ Å, suggesting a tetragonal–cubic phase transition. To investigate the phase transition of BST, differential scanning calorimetry (DSC) is undertaken under nitrogen atmosphere in aluminium crucibles at a heating rate of 5 ℃/min using a DSC Q20 from TA instruments, revealing an endothermic effect at the temperature of 303 K [Fig. 1(d)]. To verify that the phase transition is ferroelectric in nature, the temperature dependence of dielectric constant of BST was measured using a high-precision LCR meter (4282a, Agilent) at 500 Hz–1 MHz from -160 ℃ to 160 ℃ [Fig. 1(e)], exhibiting three peaks at around 176 K, 225 K and 298 K, corresponding to consecutive rhombohedral-orthorhombic-tetragonal-cubic phase transitions that have been well documented in the literature [24, 25]. An increase in dielectric dispersion with frequency can be observed in the BST ceramic, indicating that BST has diffuse phase transition owing to the substitution of Sr on the Ba site [26]. The polarization-electric field (P-E) hysteresis loops of BST ceramic were recorded on a Sawyer–Tower circuit (Precision Premier II, Radiant Technologies, Inc.) at different temperatures, revealing typical ferroelectric hysteresis at lower temperatures (Fig. 1(f)). The hysteresis loop gradually

decreases with the increased temperature, and diminishes at 330 K, further confirming the ferroelectric phase transition of BST.

III. Simulation and Experiment Results

Across ferroelectric phase transition, large variations of material properties are expected, as exhibited by dielectric constant and ferroelectric hysteresis. Particularly relevant to our study is the acoustic velocities in BST ceramic, which are measured by ultrasonic techniques, using the conventional pulse-echo technique with longitudinal and transversal ultrasonic waves. As shown in Fig. 2(a), the acoustic velocities is a function of temperature for longitudinal (c_l, square solid dots) and transverse (c_t, square solid dots) wave velocities in BST. Large increase in acoustic velocities occurs when the temperature changes from 293 K to 313 K, and outside of this range they are relatively stable, consistent with the tetragonal-cubic phase transition of BST in this temperature range. The specific wave velocities of BST are measured to be c_l = 5340 m/s, c_t = 3345 m/s for 293 K, and c_l = 6163 m/s, c_t = 4161 m/s for 313 K, respectively. The density of BST, 5400 kg/m^3 as measured by Archimedean method, is almost constant in the temperature range from 293 K to 313 K.

Furthermore, the dispersion curves of a uniform BST plate with thickness t = 0.5 mm immersed in water were calculated at temperatures 293 K and 313 K, respectively, as shown in Fig. 2(b), where A_n and S_n represent antisymmetric and symmetric Lamb modes respectively, n (0, 1, …) characterizes their orders. They clear demonstrate that Lamb modes in BST plate, which originate from the coupling of longitudinal and transverse waves via reflection from the finite boundary [29, 30], and are sensitive to the temperature. It is worth noting that the higher the frequency is, the more sensitive are A_0 and S_0 modes to the temperature, while more high order modes there are. Thus, at low frequency it would be difficult to sensor mode using different temperature since the mode shifts for different temperature are not obvious. At high frequency it also difficult to sensor a pure mode as many high modes are generated. At an intermediate frequency, if few of these low order Lamb

modes can be excited, then the BST can be used as an efficient temperature-tuned Lamb wave filter or sensor.

In order to excite and modulate Lamb mode in BST, we designed and fabricated a one-dimension PC plate model (thickness t = 0.5mm) that has one side patterned with periodical array (period p = 1.0 mm) of rectangular gratings (width w = 0.6 mm and height h = 0.3 mm), as shown in Fig. 3(a). Under the normal incidence of plane acoustic wave from the structured side, the power transmission coefficients of BST PC plate was measured in water at temperatures 293 K (blue solid line) and 313 K (red dot line), and compared to those of uniform BST plate (dash line), were shown in Fig. 3(b). The transmitted signals generated and received by a computer-controlled pulser-receiver (5800PR, Olympus) and digitized at a sampling frequency of 100 Msa/s (Octopus 822F, GAGE, Lockport, IL, USA). It is evident that the transmission for the uniform reference plate is rather low in the considered frequency range and is insensitive to the temperature change, in spite of large difference in wave velocities. This is because of the mismatch of momentum between A_0 and S_0 modes with water, as well as the mismatch of symmetry of A_1 mode with respect to the source [31]. These Lamb modes in uniform BST plate can't be excited by normal incidence [32, 33]. On the other hand, the spectra of BST PC show large transmission enhancement peaks at 2.40 MHz, 3.33 MHz and 3.55 MHz at 293 K, which change to 2.83 MHz and 3.94 MHz at 313 K. This set of experiment results thus demonstrates that the designed PC structure is necessary to excite the Lamb waves in BST [26, 27], and such Lamb wave can be tuned by the temperature change.

To further investigate the tunable transmission peaks, by using a finite-element analysis and solver software package of COMSOL Multiphysics (http://www.comsol.com/), the transmission spectra of BST PC plate and uniform BST plate were simulated at 293 K and 313 K respectively, as shown in Fig. 4(a). These frequencies of transmission peaks agree well with the experimental spectra of Fig. 3(b), even though there is a size deviation between experiment sample and designed sample. It is clearly observed that the first remarkable peak

at frequency of 2.47 MHz shifts to frequency of 2.93 MHz when the temperature is changed from 293 K to 313 K, corresponding to 18.6% frequency tenability over 20 K temperature range. Similarly, the second peak of 3.35 MHz at 293 K changes to 4.07 MHz at 313 K, a frequency shift of 21.5%. While the transmission spectra as a continuous function of temperature is simulated and shown in Fig. 4(b), which make the trend of thermal tuning more visually. As expected, the frequency trends of transmission peaks fit into the change of acoustic velocities with temperature. In addition, these velocity field distributions of five transmission enhancement peaks in Fig. 4(a) are shown in Fig. 4(c).

By comparing velocity field distribution of each peak at these two temperatures, it is revealed that the excited modes of 2.47 MHz at 293 K and 2.93 MHz at 313 K are the same, so are the excited modes of 3.35 MHz at 293 K and 4.07 MHz at 313 K. While the third peak of 3.55 MHz at 293 K in both experiment and simulation that does not appear at 313 K. As shown the last field distribution in Fig. 4(c), this peak originates from the coupling of resonance of water between gratings and Lamb mode in BST PC. Furthermore, compared Fig. 4(a) with Fig. 2(b), these frequencies of the first peak at 293 K and 313 K almost coincide with these frequencies of A_0 mode at $k = 2\pi/p$ in a uniform BST plate, while these frequencies of the second peak at 293 K and 313 K are almost the same with these frequencies of A_1 mode at $k = 0$ in a uniform BST plate. It can be explained that the Bragg scattering by the gratings on the BST PC, which folds the A_0 mode at $k = 2\pi/p$ back to $k = 0$, as well as changes the symmetry of A_1 mode, leading to these two modes matching momentum and symmetry with respect to the normal incident source[26, 27]. Thus, the first and second peaks at both 293 K and 313 K originate from the resonant excitation of the A_0 and A_1 modes that exist intrinsically in the uniform elastic plate respectively, while these Lamb modes can be effectively modulated around T_C.

In order to investigate the geometrical parameters of BST PC influence on the existence and trend of the resonant peaks, Fig 5 shows the transmission spectra for

temperature 293 K and 313 K varying with the thickness t of substrate, width w and height h of gratings, respectively, for a series of BST PC samples with other geometrical parameters identically to the aforementioned. In Fig. 5(a), the dark dash line and the white dash line give a theoretical prediction of the frequency of A_0 mode at $k = 2\pi/p$, and A_1 mode at $k = 0$ in the uniform brass plate of thickness t, respectively. As shown in Fig. 5 (a), for a small value of t, the difference of the first transmission peak in two temperature is not distinct, which is due to the corresponding A_0 mode in thin plate shifting for different temperatures are not obvious. For an intermediate value of t, as mentioned earlier these positions of the first and the second transmission peak for both two temperatures agree well with these predicted from the A_0 mode at $k = 2\pi/p$ and A_1 mode at $k = 0$ in the uniform plate, respectively. For a large value of t, multiple transmission peaks are arising and can't be distinguished effectively in two temperatures, which is due to high order Lamb modes arising in thick plate. Therefore, it is reasonable to choose an intermediate value of thickness t as 0.5 mm for the sample of BST PC substrate in experiment.

In Fig. 5(b), it is clearly shown that the width w of grating influences the frequency and shape of the first transmission peak. While as shown in Fig. 5(c), the height h of gratings affects the frequency and shape of the second transmission peak. These phenomena can be explained from the characteristic of displacement field for the A_0 and A_1 Lamb modes in a uniform plate [34]. For the A_0 mode at $k = 2\pi/p$, the longitudinal component of displacement is maximized at the surface of plate, while the transverse component is almost invariant across the plate thickness, thus the displacement of this mode is sensitive to the longitudinal displacement component. The A_1 mode at $k = 0$ in the uniform plate is the cut-off mode, while the product of frequency multiplied by plate thickness is equal to half the transverse wave velocity, thus the displacement of this mode is pure transverse. For Lamb waves in an isotropic plate, the longitudinal displacement is parallel to the surface, while the transverse displacement is normal to the surface. Thus, the A_0 mode at $k = 2\pi/p$ is more sensitive to the

8

perturbation of BST PC on the direction of parallel to the surface, i.e. the width of grating on BST substrate; The A_1 mode at $k = 0$ is more sensitive to the perturbation of BST PC on the direction of normal to the surface, i.e. the height of grating on BST substrate. Accordingly, the first and the second transmission peaks are originated from the structure-induced resonant excitation of A_0 and A_1 Lamb modes that exist intrinsically in the uniform BST plate, which are sensitive to the width w and the height h of gratings, respectively. After considering the trends of w and h influence on these two peaks in two temperature, it is reasonable to choose width as 0.6 mm and height as 0.3 mm for the grating on the surface of BST PC in experiment.

IV. Conclusion

In conclusion, we have fabricated ferroelectric ceramic materials BST with the phase transition temperature T_C at room temperature, across which the acoustical properties show substantial variation. PC consisting of periodic artificial structure on the surface of BST plate are found to be suitable for multi-frequency transmission enhancement, where transmission peaks show large thermal tunability around 20% over 20 K temperature range near room temperature. The phenomenon is attributed to the structured-induced resonant excitation of A_0 and A_1 Lamb modes that exist intrinsically in the uniform elastic plate, while these Lamb modes are sensitive to the elastic properties (longitudinal and transverse wave velocities) of plate and can be modulated by temperature in BST plate around T_C. The tunable PC via ferroelectric phase transition will pave a way to explore acoustic properties of ferroelectric materials and has promising prospects for tunable smart devices, such as temperature-tuned Lamb wave filter or sensor.

ACKNOWLEDGEMENTS

[1]   M. Kushwaha, P. Halevi, G. Martinez, L. Dobrzynski, and B. Djafari-Rouhani, Theory of acoustic band structure of periodic elastic composites, Phys. Rev. B **49**, 2313 (1994).

[2]   Y. Pennec, J. O. Vasseur, B. Djafari-Rouhani, L. Dobrzyński, and P. A. Deymier, Two-dimensional phononic crystals: Examples and applications, Surf. Sci. Rep. **65**, 229 (2010).

[3]   D. Caballero, J. Sanchez-Dehesa, C. Rubio, R. Martinez-Sala, J. Sanchez-Perez, F. Meseguer, and J. Llinares, Large two-dimensional sonic band gaps, Phys. Rev. E **60**, R6316 (1999).

[4]   X. Zhou, Y. Wang, and C. Zhang, Effects of material parameters on elastic band gaps of two-dimensional solid phononic crystals, J. Appl. Phys. **106**, 014903 (2009).

[5]   A. Khelif, P. Deymier, B. Djafari-Rouhani, J. Vasseur, and L. Dobrzynski, Two-dimensional phononic crystal with tunable narrow pass band: Application to a waveguide with selective frequency, J. Appl. Phys. **94**, 1308 (2003).

[6]   Y. Pennec, B. Djafari-Rouhani, J. Vasseur, A. Khelif, and P. Deymier, Tunable filtering and demultiplexing in phononic crystals with hollow cylinders, Phys. Rev. E **69**, 046608 (2004).

[7]   K. Bertoldi and M. Boyce, Mechanically triggered transformations of phononic band gaps in periodic elastomeric structures, Phy. Rev. B **77** 052105 (2008).

[8]   X. Y. Zou, Q. Chen, B. Liang, and J. C. Cheng, Control of the elastic wave bandgaps in two-dimensional piezoelectric periodic structures. Smart Mater. Struct. **17**, 015008 (2008).

[9]   J. Y. Yeh, Control analysis of the tunable phononic crystal with electrorheological material. Physica B: Condens. Matter. **400**, 137 (2007).

[10]   J. F. Robillard, O. B. Matar, J. Vasseur, P. Deymier, M. Stippinger, A. C. Hladky-Hennion, Y. Pennec, and B. Djafari-Rouhani, Tunable magnetoelastic phononic crystals, Appl. Phys. Lett. **95**, 124104 (2009).

[11]   J. Vasseur, O. B. Matar, J. F. Robillard, A. C. Hladky-Hennion, and P. Deymier, Band structures tunability of bulk 2D phononic crystals made of magneto-elastic materials, AIP Adv. **1**, 041904 (2011).

[12]   Z. Xu, F. Wu, and Z. Guo, Shear-wave band gaps tuned in two-dimensional phononic crystals with magnetorheological material. Solid State Commun, **154**, 43 (2013).

[13]   Y. Wang, F. Li, K. Kishimoto, Y. Wang, and W. Huang, Elastic wave band gaps in magnetoelectroelastic phononic crystals, Wave Motion **46**, 47 (2009).

[14]   Y. Wang, F. Li, W. Huang, X. Jiang, Y. Wang,, and K. Kishimoto, Wave band gaps in two-dimensional piezoelectric/piezomagnetic phononic crystals, Int. J. Solids Struct. **45**, 4203 (2008).

[15]   A. Sato, Y. Pennec, N. Shingne, T. Thurn-Albrecht, W. Knoll, M. Steinhart, B. Djafari-Rouhani, and G. Fytas, Tuning and switching the hypersonic phononic properties of elastic impedance contrast nanocomposites, ACS nano **4**, 3471 (2010).

[16]   W. Cheng, J. Wang, U. Jonas, G. Fytas, and N. Stefanou, Observation and tuning of hypersonic bandgaps in colloidal crystals, Nat. Mater. **5**, 830 (2006).

[17]   H. Tang, C. Luo, and X. Zhao, Tunable characteristics of a flexible thin electrorheological layer for low frequency acoustic waves, J. Phys. D: Appl. Phys. **37**, 2331 (2004).

[18]   K. Jim, C. Leung, S. Lau, S. Choy, and H. Chan, Thermal tuning of phononic bandstructure in ferroelectric ceramic/epoxy phononic crystal, Appl. Phys. Lett. **94**, 193501 (2009).

[19]   Y. Yao, F. Wu, X. Zhang, and Z. Hou, Thermal tuning of Lamb wave band structure in a two-dimensional phononic crystal plate, J. Appl. Phys. **110**, 123503 (2011).

[20]   Y. Cheng, X. Liu, and D. Wu, Band structures of phononic-crystal plates in the form of a sandwich-layered structure, J. Acoust. Soc. Am. **130**, 2738 (2011).

[21]   Z. Bian, W. Peng, and J. Song, Thermal tuning of band structures in a one-dimensional phononic crystal, J. Appl. Mech.-T. ASME **81**, 041008 (2014).

[22]   C. Fu, C. Yang, H. Chen, Y. Wang, and L. Hu, Microstructure and dielectric properties of $Ba_xSr_{1-x}TiO_3$ ceramics, Mater. Sci. Eng. B. **119**, 185 (2005).

[23]   O. Thakur, C. Prakash, and D. Agrawal, Dielectric behavior of $Ba_{0.95}$ $Sr_{0.05}TiO_3$ ceramics sintered by microwave, Mater. Sci. Eng. B. **96**, 221 (2002).

[24]   L. Benguigui, Disordered ferroelectrics: $Ba_xSr_{1-x}TiO_3$ single crystals, Phys. Status Solidi A **46**, 337 (1978).

[25]   K. Bethe and F. Welz, Preparation and properties of (Ba, Sr) TiO_3 single crystals, Mater. Res. Bull. **6**, 209 (1971).

[26]   Z. He, H. Jia, C. Qiu, S. Peng, X. Mei, F. Cai, P. Peng, M. Ke, and Z. Liu, Acoustic Transmission Enhancement through a Periodically Structured Stiff Plate without Any Opening, Phys. Rev. Lett. 105, 074301 (2010).

[27]   H. Jia, M. Ke, C. Li, C. Qiu, and Z. Liu, Unidirectional transmission of acoustic waves based on asymmetric excitation of Lamb waves, Appl. Phys. Lett. 102, 153508 (2013).

[28]   A. Moreno-Gobbi, D. Garcia, J. A. Eiras, and A. S. Bhalla, Study by ultrasonic techniques of the phase diagram of BST ceramic family mainly for high Sr concentrations, Ferroelectrics **337**, 197 (2006).

[29]   H. Lamb, On waves in an elastic plate, Proc. R. Soc. London, Ser. A **93**, 114 (1917).

[30]   J. Wu and Z. Zhu, The propagation of Lamb waves in a plate bordered with layers of a liquid, J. Acoust. Soc. Am. **91**, 861 (1992).

[31]   F. L. Hsiao, A. Khelif, H. Moubchir, A. Choujaa, C. C. Chen, and V. Laude, Complete band gaps and deaf bands of triangular and honeycomb water-steel phononic crystals, J. Appl. Phys. **101**, 044903 (2007).

[32]   M. Castaings and P. Cawley, The generation, propagation, and detection of Lamb waves in plates using air-coupled ultrasonic transducers. J. Acoust. Soc. Am. **100**, 3070 (1996).

[33]   V. Dayal and V.K. Kinra, Leaky Lamb Waves in an Anisotropic Plate. I: An Exact Solution and Experiments. J. Acoust. Soc. Am. **85**, 2268 (1989).

[34]   R. Daniel, and D. Eugene, Elastic Waves in Solids I: Free and Guided Propagation, Springer, (2000). P318.
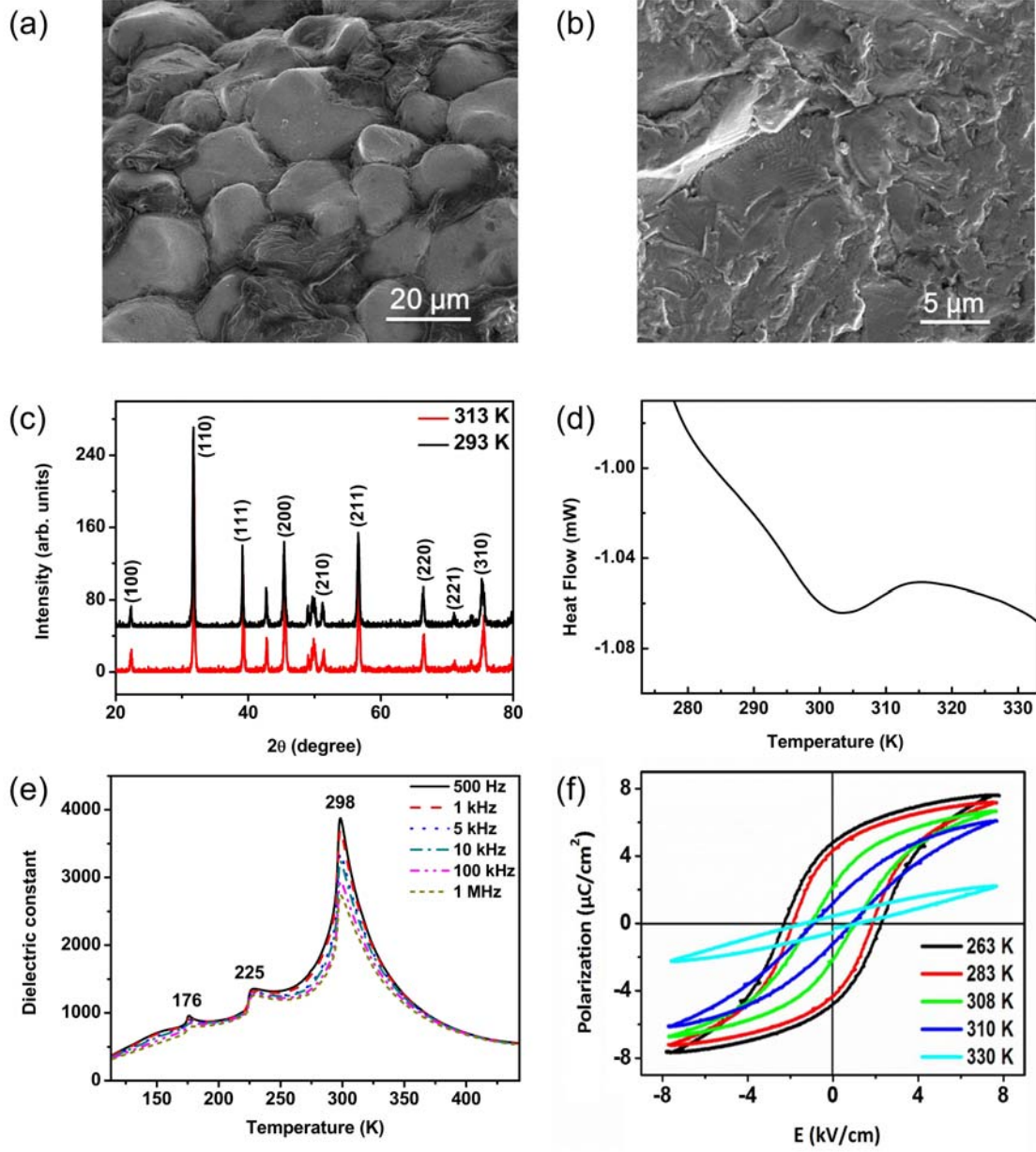
FIG. 1. Ferroelectric phase transition of BST. (a) Surface SEM micrographs of BST ceramic. (b) Cross-section SEM micrographs. (c) XRD patterns at temperature of 293 K and 313 K. (d) DSC curve. (e) the variation in the dielectric constant as a function of temperature at the frequency from 500 Hz to 1 MHz. (f) Ferroelectric hysteresis loops at temperatures above and below T_C.
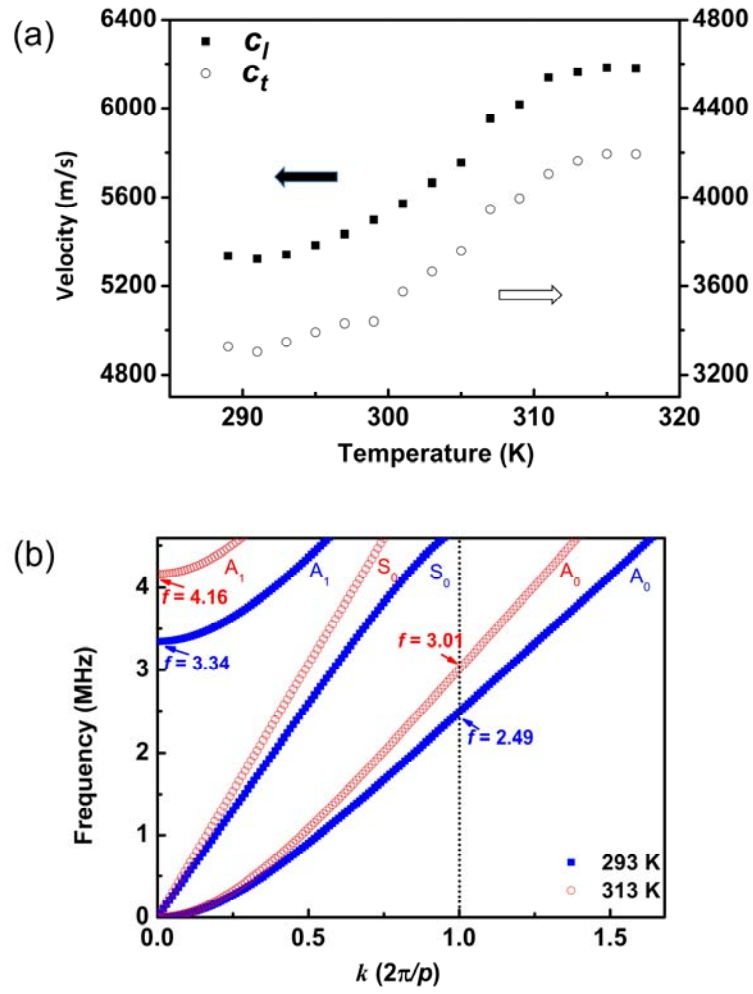
FIG. 2. (a) Longitudinal and transverse wave velocities measured at temperatures range from 289 K to 317 K. (b) Dispersion curves of Lamb wave in a uniform BST ceramic of thickness t = 0.5 mm immersed in water at 293 K (blue square dots) and 313 K (red circle dots).
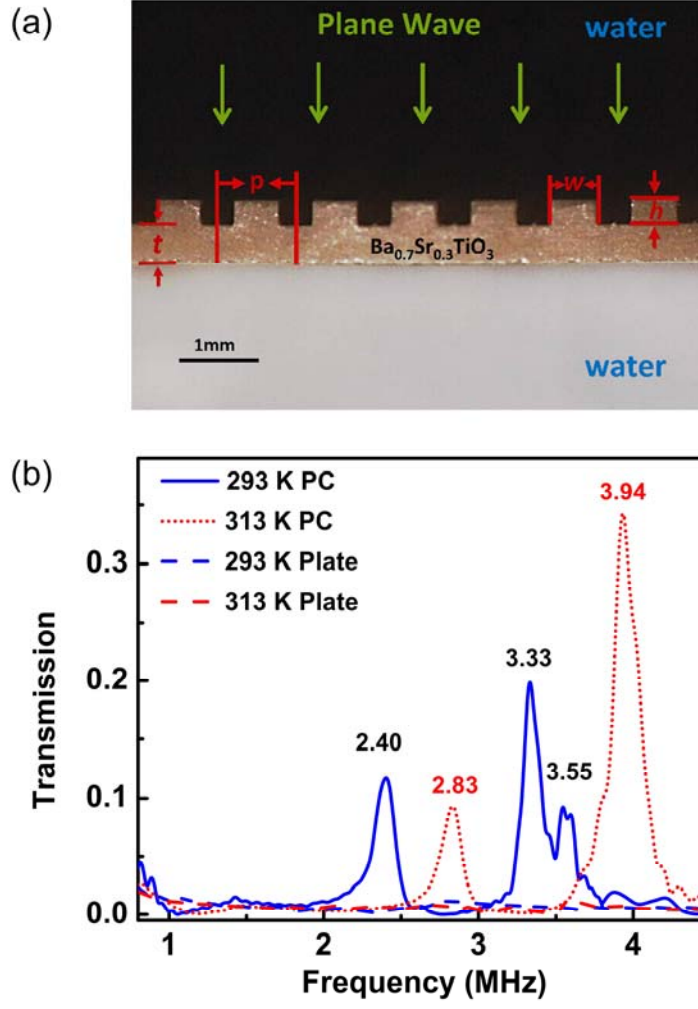
FIG. 3. (a) Schematic representation and photograph of the PC plate. (b) The experimental power transmission coefficients of PC (solid line and dot line) and uniform BST plate (dash line) at 293 K (blue) and 313 K (red).
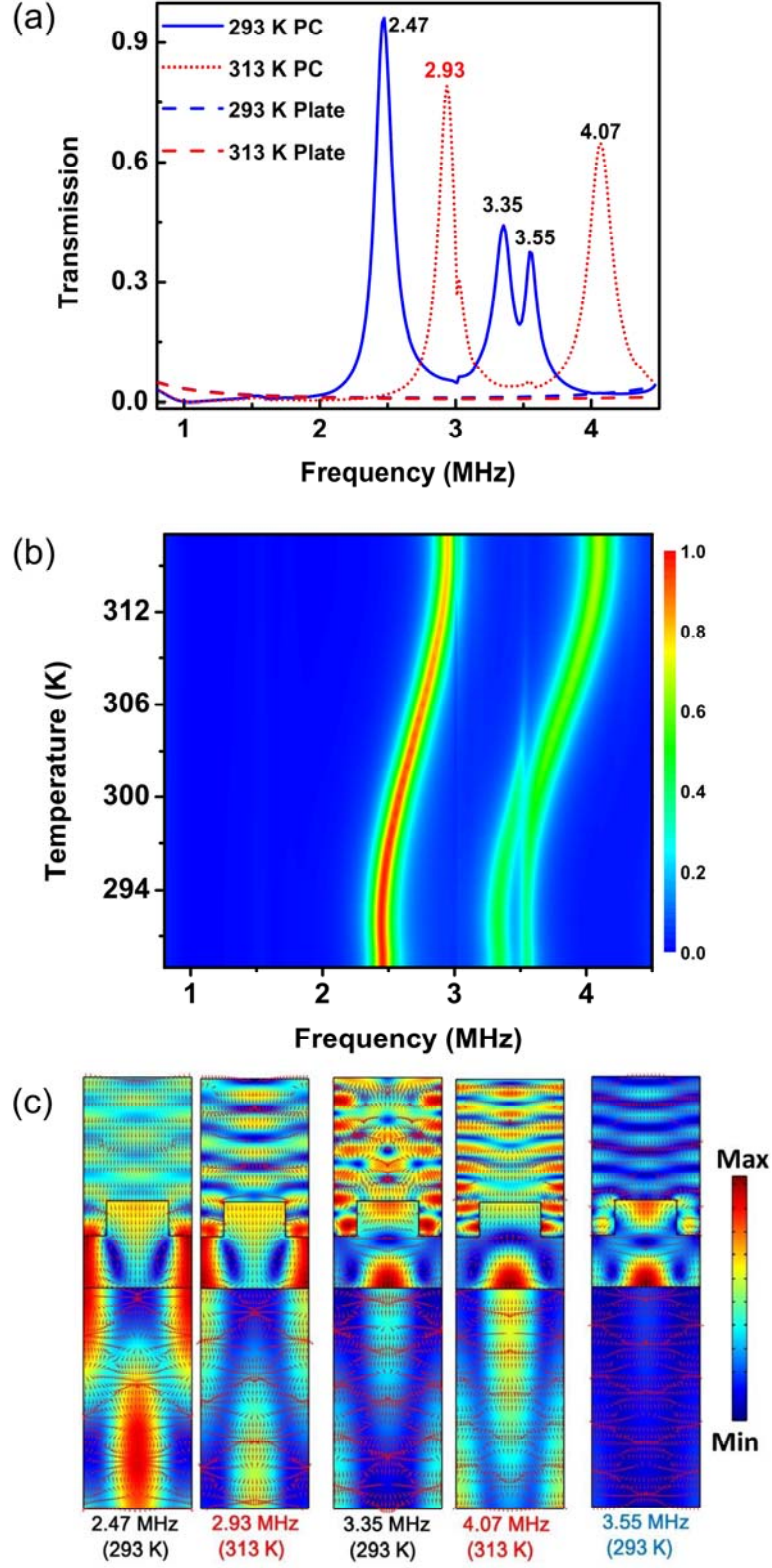
FIG. 4. (a) The simulated power transmission coefficients of BST PC (solid line and dot line) and uniform BST plate (dash line) at 293 K (blue) and 313 K (red). (b) Transmission spectra

of BST PC as a function of temperature from 289 K to 317 K. (c) The simulated velocity field distribution of one unit cell of BST PC at 2.47 MHz, 3.35 MHz and 3.55 MHz at 293 K, 2.93 MHz and 4.07 MHz at 313 K, both the amplitude field (color variations) and the vector field (arrows) are provided.
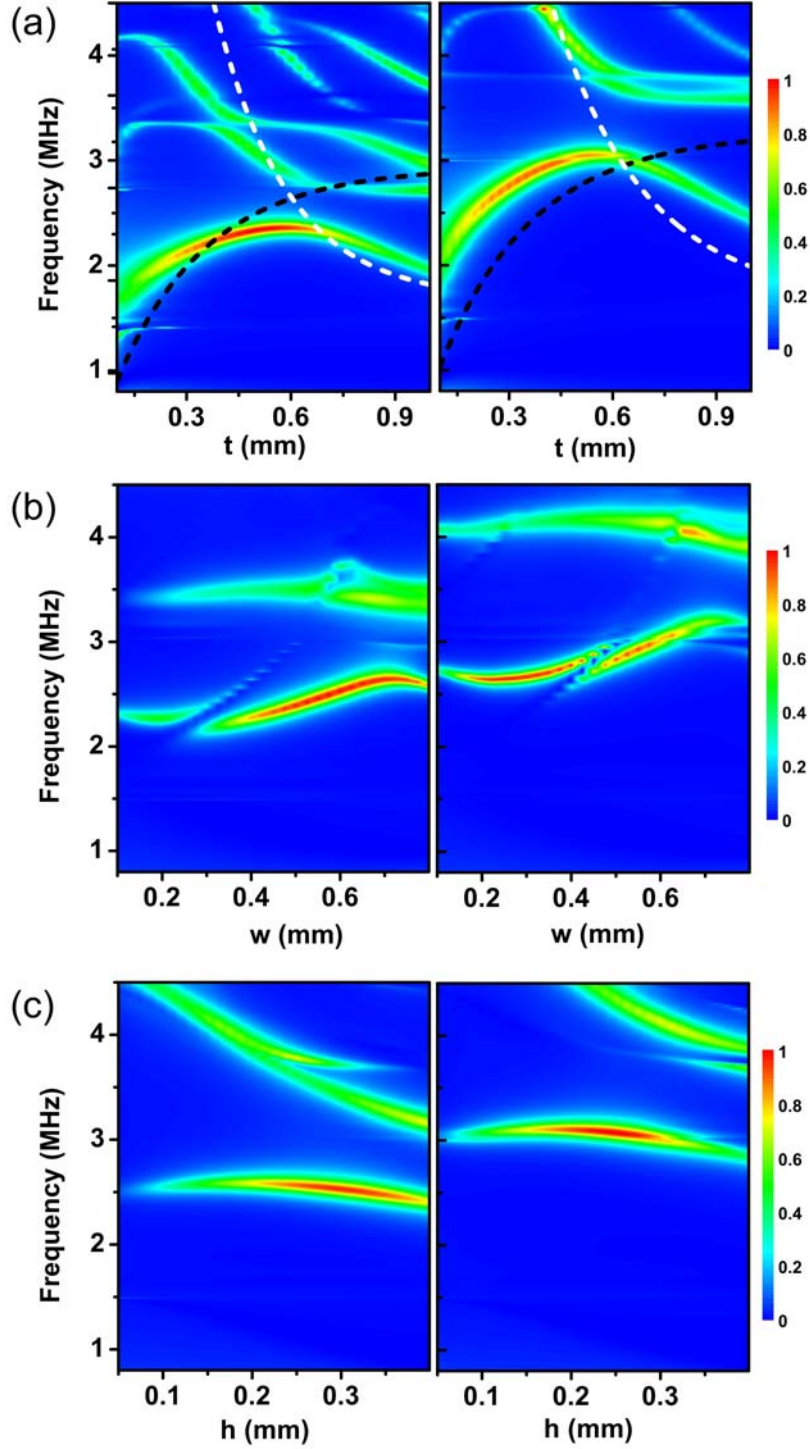
FIG. 5. Transmission spectra versus geometric parameters (thickness t of BST substrate (a), width w (b) and height h (c) of gratings) at 293 K (left) and 313 K (right) for a series of BST PC samples with other geometric parameters identically to the aforementioned. In (a), the

dark dash line and the white dash line give a theoretical prediction of the frequency of A_0 mode at $k = 2\pi/p$, and A_1 mode at $k = 0$ in the uniform brass plate of thickness t, respectively.